The importance of high precision in the evaluation of U-Pb zircon age spectra

Gaynor, Sean; Ruiz, Mélissa; Schaltegger, Urs

How to cite

GAYNOR, Sean, RUIZ, Mélissa, SCHALTEGGER, Urs. The importance of high precision in the evaluation of U-Pb zircon age spectra. In: Chemical geology, 2022, p. 120913. doi: 10.1016/j.chemgeo.2022.120913

This publication URL: https://archive-ouverte.unige.ch/unige:160899

Publication DOI: 10.1016/j.chemgeo.2022.120913

Chemical Geology xxx (xxxx) 120913

Contents lists available at ScienceDirect

Chemical Geology

journal homepage: www.elsevier.com/locate/chemgeo

The importance of high precision in the evaluation of U-Pb zircon age spectra

Sean P. Gaynor *, Mélissa Ruiz, Urs Schaltegger

Department of Earth Sciences, University of Geneva, 1205 Geneva, Switzerland

ARTICLE INFO

Editor: Catherine Chauvel

Keywords:
U-Pb Geochronology
Zircon
ID-TIMS

ABSTRACT

We present high-precision isotope dilution-thermal ionization mass spectrometry (ID-TIMS) U-Pb zircon data from the Carboniferous Punteglias granodiorite from the Central Alpine basement in the Aar massif in Switzerland. These analyses yield complex age spectra consisting of both concordant and normally discordant dates, which form a linear array indicative of mixing of two age components within individual zircon crystals. While the upper intercept age reflects zircon growth during Variscan magmatism, the lower intercept of 24 ± 11 Ma is coincident with the Alpine orogeny. There is poor evidence from cathodo-luminescence imagery that magmatic zircon may have younger overgrowths, therefore, we pretreated an aliquot of zircon with physical abrasion followed by chemical abrasion to remove any potential later zircon overgrowths, and to directly date the initial magmatic domains of the zircon. This pretreatment significantly reduced age dispersion and yielded an age of 335.479 ± 0.041 Ma for the crystallization of zircon in the Punteglias granodiorite. Due to the effectiveness of this pretreatment, we interpret that the magmatic zircon was overgrown with younger domains during the Alpine orogeny. Detangling the observed complications in the Punteglias granodiorite zircons was largely possible due to the particularly high analytical precision of the ID-TIMS U-Pb dates that made it possible to detect discordance between the $^{206}Pb/^{238}U$ and $^{207}Pb/^{235}U$ systems. Lower-precision U-Pb ID-TIMS dates would not allow identification of such a two-component mixture and lead to analytically concordant points spreading over 10^5 to 10^6 years, and potentially leading to erroneous scientific interpretation. As an example, we model two hypothetical situations of simple mixing of two age components in the U-Pb concordia space to demonstrate the effect of precision on the ability to accurately interpret geological models from complicated age spectra. Combining these new high-precision data and modeling results highlights the importance of choosing the optimal, physical and/or chemical sample pre-treatment and the challenge of accurately interpreting complicated U-Pb data in terms of crystallization age.

1. Introduction

Precise and accurate U-Pb geochronology is important for resolving many problems in Earth sciences, such as establishing synchrony or causality between different geological events through absolute dating. The isotope dilution, thermal ionization mass spectrometry (ID-TIMS) U-Pb technique is generally considered to be the "gold standard" of geochronology due to its high analytical precision and accuracy. Mostly applied to the mineral zircon ($ZrSiO_4$), U-Pb dates are known to be highly reliable, because zircon tends to be robust in the face of post-crystallization alteration and system disturbance. Another class of techniques such as laser ablation, inductively coupled plasma mass spectrometry (LA-ICPMS) or secondary ion mass spectrometry (SIMS) are capable of highly spatially resolved U-Pb geochronology, targeting discrete, previously imaged or chemically characterized volumes of zircon crystals through in-situ analysis. However, they require well characterized reference materials to calibrate mass and elemental discrimination correction factors and are less precise.

A series of advancements in chemical and mass spectrometric techniques used in ID-TIMS geochronology have improved the precision and accuracy below 0.1% for single crystal $^{206}Pb/^{238}U$ ages. Among these are the chemical abrasion treatment to mitigate Pb-loss (e.g., Widmann et al., 2019), the introduction of calibrated EARTHTIME (^{202}Pb-)^{205}Pb-^{233}U-^{235}U (ET535 and ET2535) tracer solutions (e.g., Condon et al., 2015), lowering of procedural Pb blanks to 100–300 fg (e.g., Schaltegger et al., 2021a) and improvement of collector sensitivity through the development of higher stability multipliers and high-ohmic resistor based or capacitive-based Faraday technologies (e.g.,

* Corresponding author.
E-mail address: sean.gaynor@unige.ch (S.P. Gaynor).

https://doi.org/10.1016/j.chemgeo.2022.120913
Received 28 January 2022; Received in revised form 1 May 2022; Accepted 9 May 2022
0009-2541/

von Quadt et al., 2016; Szymanowski and Schoene, 2020). This increased precision, especially when working with small sample volumes, commonly yields protracted age spectra, wherein several individual zircon dates of the same sample do not all overlap within uncertainty. Interpretation of such complicated high-precision age spectra has led to novel conceptual models of eruption mechanics (e.g., Wotzlaw et al., 2013; Curry et al., 2021), batholith formation (e.g., Samperton et al., 2015; Gaynor et al., 2019a), porphyry development (e.g., Tapster et al., 2016; Large et al., 2021), thermochronology of igneous rocks (e.g., Samperton et al., 2017), and the dynamics of large igneous provinces (e.g., Schoene et al., 2019; Gaynor et al., 2022). However, for these models to accurately reflect natural processes, it is crucial that the U-Pb data are carefully evaluated and correctly interpreted.

Geological interpretations of protracted zircon spectra commonly invoke several mechanisms for their origin: (1) Pb-loss leading to ages that postdate crystallization, (2) prolonged zircon growth within a single magma reservoir, referred to as autocrysts, (3) inheritance of zircon and/or domains of zircon from previous magma pulses, referred to as antecrysts, (4) inheritance of ancient zircon from either wall rock or the anatectic source, referred to as xenocrysts (e.g., Miller et al., 2007). Mechanisms (2) to (4) involve mixing of multiple ages of crystallization in a single crystal, which are in turn lumped together into a single dissolved analyte prior to analysis. Identifying the nature of each zircon crystal before or after analysis either requires additional geochemical information, or imaging of sectioned crystals, and relies strictly upon accurate interpretation of individual ages and of the cause of age dispersion.

To investigate the possible complications in zircon age spectra and how different techniques can resolve them, we analyzed a suite of zircon crystals from the Punteglias granodiorite from the Alpine basement (Aar Massif, Switzerland), using several analytical techniques and pretreatment methods. This sample had previously been analyzed by Schaltegger and Corfu (1992), however there have been significant improvements in U-Pb analytical methods since those data were generated. Zircons from the selected sample are relatively large, have produced significant in-growth of radiogenic Pb (Pb*), and are therefore capable of providing the highest precision U-Pb dates, more precise than many typical samples of interest. Preliminary CA-ID-TIMS analysis of these grains yielded complicated and discordant spectra, which required a physical abrasion step prior to chemical abrasion in order to remove the margins of the grain. This exercise revealed complicated zircon systematics that may go undetected in lower-precision data sets. Altogether, these data highlight the need for careful assessment of complicated U-Pb dates, in order to ensure a more accurate interpretation of a geologic age.

2. Geological setting

The Aar Massif is one of the crystalline external massifs of the Alpine basement, exposed as an elongated belt of rocks which formed during Variscan and pre-Variscan orogenic cycles (e.g., von Raumer et al., 2013). The Variscan orogeny juxtaposed the continental margins of Laurussia and Gondwana during oceanic subduction in the Devonian and continental collision in the Carboniferous. During the waning periods of this orogeny, extensive melting of lithospheric mantle and lower crust in a strongly overthickened orogenic root occurred in an extensional to transtensional tectonic setting, leading to the intrusion of intermediate to felsic magmas into the middle and upper crust. The late-Variscan batholiths emplaced in general during distinct pulses of lithospheric extension, exhumation and decompressional melting from 340 to 290 Ma ago, with some degree of diachroneity in different Variscan domains, e.g., the Bohemian Massif (Schulmann et al., 2014) or the French Massif Central (Vanderhaeghe et al., 2020).

The Aar batholith formed during multiple additions of melts between 348 and 298 Ma (Schaltegger and Corfu, 1992, 1995). One conspicuous pulse consisted of ca. 332–335 Ma shoshonitic diorites, monzonites, syenites, granodiorites and granites, (e.g., Schaltegger et al., 1991; Schaltegger, 1997), which are characterized by non-radiogenic initial Hf isotope compositions and interpreted as the products of melting of a strongly enriched lithospheric mantle source that partly underwent crustal contamination (Schaltegger and Corfu, 1992). High-K intermediate to mafic rocks termed “vaugnerites” or “durbachites” are found along the entire strike of the Variscan root zone (e.g., von Raumer et al., 2013; Janoušek et al., 2020). One member of this group of rocks is the Punteglias granodiorite, which is exposed as a lens-shaped body over approximately 10 km^2 in the southeastern margin of the Aar Massif (Fig. 1). It is a heterogeneous intrusion, ranging from monzodiorite to granodiorite and granite (Seeman, 1975; Schaltegger et al., 1991).

The rocks of the Punteglias intrusion were subject to overprinting during the Alpine orogeny, with alteration and replacement of magmatic feldspars, biotite and amphibole under greenschist facies condi-

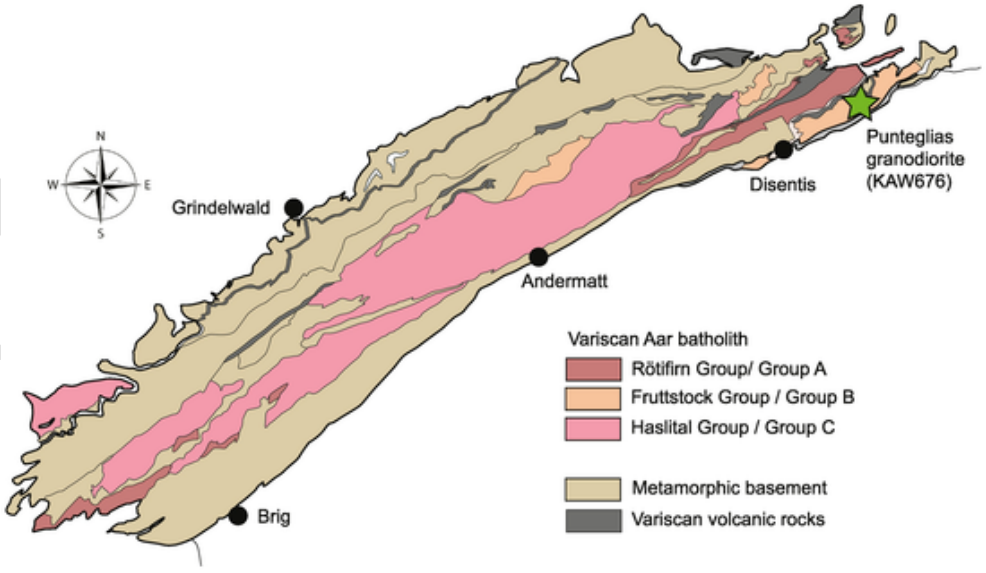

Fig. 1. Geologic map of the Aar massif, showing the extent of the pulsed Carboniferous magmatism of the Aar batholith and highlighting the location of sample KAW676 of the Punteglias granodiorite presented in this study (modified after Berger et al., 2017).

tions, with a temperature peak of 450 °C prior to 20 Ma (Challandes et al., 2008; Rolland et al., 2009; Janots and Rubatto, 2014). Traditionally, discordant U-Pb ages from untreated and physically abraded bulk zircon aliquots from late Variscan intrusive rocks were interpreted to be the result of Pb-loss during this metamorphic overprint (e.g., Schaltegger and von Quadt, 1990; Schaltegger and Corfu, 1992).

3. Methods

Zircon of sample KAW676 was separated using standard procedures and dated using physical abrasion ID-TIMS techniques by Schaltegger and Corfu (1992). The original sample consisted of aproximately 25 kg of rock, and yielded large quantities of zircon. The analyzed zircon material was taken from a fraction that was non-magnetic at 1° side slope on a Frantz magnetic separator at maximum magnet intensity.

Three aliquots of zircon were picked from the separate, and two underwent physical abrasion (PA) for 5 h (676PA) and 12 h (676PA2) in the presence of minor amounts of pyrite to obtain a polished surface and remove the outer crystalline domains. These two latter aliquots were washed in an ultrasonic bath with 7 M HNO_3, and then H_2O. All three aliquots of zircon were subsequently annealed in a muffle furnace at 900 °C for 48 h (Mundil et al., 2004). The annealed grains were chemical abraded at 210 °C for 12 h in concentrated HF in 3 ml Savillex vials placed in a Parr digestion vessel (Mattinson, 2005; Widmann et al., 2019). The grain fragments remaining after chemical abrasion were then leached on a hotplate at 80 °C in 6 N HCL overnight, followed by further cleaning through four rounds of 7 N HNO_3 in combination with ultrasonication. Individual cleaned zircon crystals were then loaded into individual 200 µl Savillex microcapsules, spiked with the EARTHTIME $^{202}Pb + ^{205}Pb + ^{233}U + ^{235}U$ tracer solution (calibration version 3; Condon et al., 2015; McLean et al., 2015) and dissolved with about 70 µl HF and trace HNO_3 in a Parr digestion vessel at 210 °C for 48 h. Following dissolution, the samples were dried down and converted to a chloride by placing them back in the oven overnight in 6 N HCl. The samples were then dried down again and re-dissolved in 3 N HCl and purified to U and Pb through anion exchange column chromatography (Krogh, 1973). Once purified, the U and Pb fractions were combined in cleaned 7 ml Savillex beakers and dried down with trace H_3PO_4, prior to loading on outgassed zone-refined Re ribbon filaments with a Si-gel emitter. U and Pb isotope analyses were completed on an IsotopX Phoenix TIMS machine at the University of Geneva (Switzerland). Lead measurements were made in dynamic mode using a Daly photomultiplier, and U was measured as an oxide in static mode using Faraday cups coupled to 10^{12} Ω resistors. The $^{18}O/^{16}O$ oxygen isotope ratio in uranium oxide was assumed to be 0.00205 based on previous measurements of the U500 standard. Mass fractionation of Pb was corrected using a $^{202}Pb/^{205}Pb$ ratio of 0.99506 and U was corrected using the composition of the spike solution (Condon et al., 2015). The abundance of U was calculated using a sample composition $^{238}U/^{235}U$ ratio of 137.818 ± 0.045 (2σ; Hiess et al., 2012). All common Pb was considered laboratory blank and was corrected using the long-term isotopic composition of the Pb blank at the University of Geneva (Schaltegger et al., 2021a). All data were processed with the Tripoli and Redux U-Pb software packages (Bowring et al., 2011; McLean et al., 2011). All ages were corrected for initial ^{230}Th disequilibrium in the melt using a U/Th ratio of the magma of 3.5. Earthtime ET100Ma standard solution analyzed during the period of these analyses yielded a $^{206}Pb/^{238}U$ date of 100.1785 ± 0.0064 Ma (MSWD = 2.7; n = 15), within uncertainty of the recently reported inter-laboratory calibrated value of 100.173 ± 0.003 Ma for this solution (Schaltegger et al., 2021a; database at DOI: 10/gk53tk). The uncertainty of weighted mean $^{206}Pb/^{238}U$ ages is given in the X/Y/Z notation, where X = analytical error only/ Y = with uncertainty of spike calibration added/Z = with uncertainty of decay constants added (Schoene et al., 2019).

4. Results

All CA-ID-TIMS zircon analyses yielded Carboniferous Th-corrected $^{206}Pb/^{238}U$ ages between 335.5 and 314 Ma (Table S1), however dispersion within the age spectra varied significantly between aliquots, and many analyses are normally discordant (Fig. 3). Fourteen zircon analyses from the aliquot which were chemically abraded but did not undergo physical abrasion (aliquot 676) yielded $^{206}Pb/^{238}U$ ages between 313.95 ± 0.10 Ma and 334.655 ± 0.081 Ma. Only 5 of the 14 results are concordant, the remaining are normally discordant. Eight zircon analyses from aliquot 676PA, which underwent a light physical abrasion of 5 h prior to chemical abrasion, yielded $^{206}Pb/^{238}U$ ages between 323.73 ± 0.12 Ma and 334.509 ± 0.099 Ma. Only 6 of the 8 grains analyzed are concordant, the remaining two grains are normally discordant. Ten zircon analyses from aliquot 676PA2, which underwent moderate physical abrasion of approximately 12 h prior to chemical abrasion, yielded $^{206}Pb/^{238}U$ ages between 332.046 ± 0.081 Ma and 335.503 ± 0.078 Ma. All ten analyses were concordant. Zircon analyses from all three aliquots yielded $^{207}Pb/^{206}Pb$ ages around 335 Ma.

5. Discussion

5.1. Interpreting a crystallization age of the punteglias granodiorite

Zircon geochronology from all aliquots of the Punteglias granodiorite analyzed by ID-TIMS yield complicated age spectra, commonly with little to no overlap between individual analyses and showing significant age dispersion. As a result, a simple interpretation of the zircon crystallization age of this sample is not possible. Instead, because of the complications of these data and their high precision, they serve as an excellent example to illustrate complications that can appear in U-Pb zircon data sets.

While there is significant scatter in the CA-ID-TIMS $^{206}Pb/^{238}U$ ages of the grains analyzed from the Punteglias granodiorite, combining all analyses yields a linear fit within concordia space, indicating an upper intercept of 334.6 ± 0.60 Ma and a lower intercept of 24 ± 11 Ma (MSWD = 5.2, n = 32; Fig. 3). Given the abundances of 260–1100 ppm for both Th and U in zircon from sample 676 (Ruiz et al., n.d.), these zircon crystals only received time integrated alpha doses of 8–14 × 10^{17} α/g, which indicates it is unlikely that they became metamict due to radiation damage (e.g., Murakami et al., 1991; Pidgeon, 2014). Therefore, the observed younger ages are unlikely to reflect Pb-loss, particularly given the twelve hour, 210 °C chemical abrasion pretreatment all ID-TIMS analyses received for this study. Instead, we interpret the observed linear array as being indicative of mixing of two discrete zircon age domains within individual grains, and these two intercept ages reflecting regional geologic events. The upper intercept corresponds to the first magmatic pulse of Late Variscan melts (group A in Fig. 1; Schaltegger and Corfu, 1992). The lower intercept age points to the Alpine metamorphic overprint, which reached upper greenschist conditions in the region between approximately 17–22 Ma and causing significant fluid alteration to the region and variably deforming the granitic basement (e.g., Marquer and Burkhard, 1992; Challandes et al., 2008; Rolland et al., 2009; Berger et al., 2017; Wehrens et al., 2017). From these data we infer epitaxial growth of Alpine rims over existing zircon crystals, not readily visible in CL images (Fig. 2; Fig. S1).

Mixing of two discrete age domains (metamorphic overgrowth onto igneous zircon, or magmatic autocrystic zircon overgrowing antecrystic or xenocrystic cores) can fundamentally bias an age determination if it remains unresolved. In our example here, overgrowth of Variscan igneous zircon during Alpine metamorphism obfuscates the crystallization age of the Punteglias granodiorite without proper pre-treatment. As these rims are not more than 5–10 µm thick and are easily overlooked in CL-imagery (Fig. 2), even small volumes of Alpine rim do-

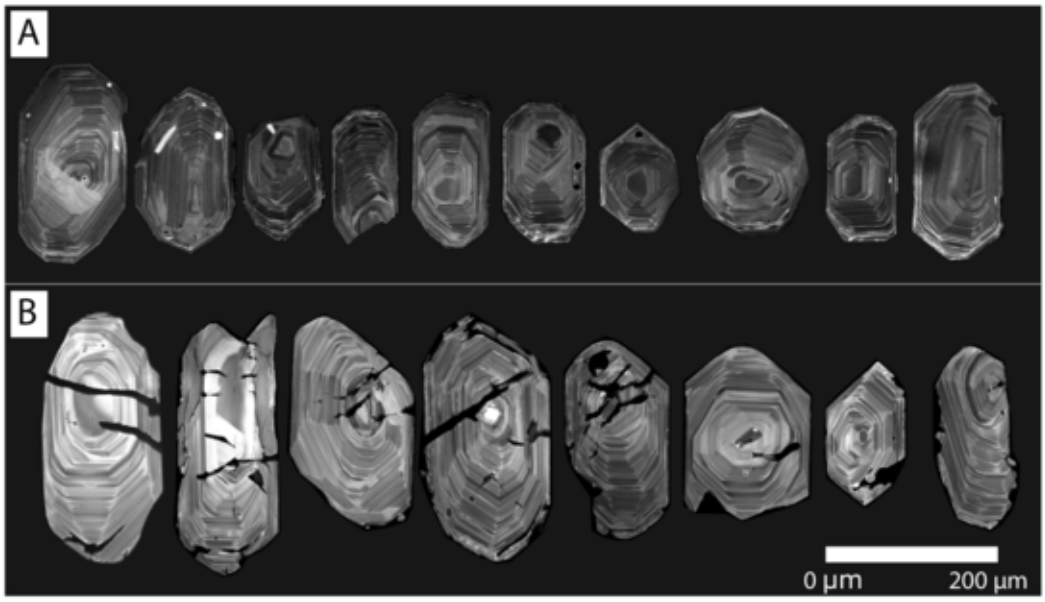

Fig. 2. Cathodoluminescence imagery of representative zircon from sample KAW676, including grains with (A) no chemical pre-treatment and (B) thermally annealing and 12 h of chemical abrasion at 210 °C. Several grains host poorly visible epitactic rims, which are potentially younger zircon overgrowths. Grains which have undergone chemical abrasion do not appear to have preferentially dissolved exterior domains, as many grains are still euhedral to subhederal. They, however, include many channelized dissolution pathways, likely from the preferential dissolution of mineral inclusions or metamict domains within zircon grains, as the chemically abraded zircons do not host the mineral inclusions observed in the untreated grains.

mains can significantly affect the bulk zircon age, causing normally discordant ages. Therefore, on aliquots 676PA and 676PA2 we utilized physical abrasion prior to thermal annealing and chemical abrasion, to remove exterior domains that may have crystallized during Miocene metamorphism. These two aliquots have significantly smaller variations in discordance, and the more intensely physically abraded grains (676PA2) yielded only concordant analyses, a significantly suppressed age range, and a group of six zircon with overlapping $^{206}Pb/^{238}U$ ages. As a result, we interpret that the discordance is the result of Alpine zircon overgrowths, and that physical abrasion was largely effective in removing these younger zircon domains. There are also no anomalously older analyses within any of the three aliquots, the oldest grains analyzed form a coherent population, so we also interpret this zircon did not crystallize with any significant inheritance.

The statistically equivalent older population of aliquot 676PA2 yielded a $^{206}Pb/^{238}U$ weighted mean age of 335.479 ± 0.041/0.096/0.37 Ma (n = 4; MWSD = 0.27; analyses Z10, Z9, Z3, Z6; Table S1), and is interpreted to most accurately reflect the crystallization of the Punteglias granodiorite. Including the two overlapping, younger analyses Z4 and Z7 into this weighted mean yields a more precise weighted mean calculation (335.440 ± 0.035/0.094/0.37 Ma), but it also yields a MWSD of 2.8, indicative that these six analyses do not represent a single population. Including these, the weighted mean age becomes younger by 39 kyr, highlighting how easy it is to shift a calculated age out of accuracy by inappropriately selecting data for weighted mean age calculation. It is likely that these two grains still contain minimal volumes of Alpine crystallographic domains.

Several studies have highlighted the potential problems with chemical abrasion preferentially dissolving exterior domains of the grain, and therefore biasing CA-ID-TIMS datasets artificially towards older ages (e.g., Samperton et al., 2015; Rivera et al., 2016; Curry et al., 2021). In this example, the subtle Alpine overgrowths are still present in the data set for chemically abraded zircon, because chemical abrasion preferentially dissolves more internal damaged and metamict zircon domains and mineral inclusions rather than preferentially the outer grain (Fig. 2B). If chemical abrasion preferentially dissolved exterior crystallographic domains there should not be any significant difference in the data generated from physically abraded and non-physically abraded zircon aliquots.

5.2. Implications for high-precision U-Pb interpretations

The CA-ID-TIMS results from the Punteglias granodiorite serve as an example how mixing of zircon domains crystallized within individual grains during two temporally separated geologic events can lead to discordant data. Similar data may erroneously be interpreted in terms of prolonged zircon growth within a single magma system (autocrysts), or zircon growth in an individual magma and the incorporation of variably older components (e.g., antecrysts or xenocrysts). Zircon dates that analytically overlap with concordia indicate agreement between their $^{206}Pb/^{238}U$ and $^{207}Pb/^{235}U$ dates within uncertainty, suggesting that the analysis does not reflect incorporation of an age component significantly different than the bulk of the grain, i.e., does not reflect xenocrystic inheritance. Therefore, it is common for extended concordant age spectra to be interpreted as reflecting the magmatic history of an individual sample implying protracted autocrystic growth and/or recycling of antecrysts. These different interpretations may lead to contrasting genetic models for intermediate to high silica magma systems.

However, the degree of overlap with the concordia uncertainty band for an individual analysis is rooted in analytical uncertainty; $^{207}Pb/^{235}U$ ages tend to be less precise than $^{206}Pb/^{238}U$ ages due to the lower amount of radiogenic ^{207}Pb relative to ^{206}Pb (Fig. 4). Overall, the precision on individual zircon ages is a function of analyte material and lab practices, any common Pb present in analysis (e.g., as procedural lab blank) is overwhelmed as the zircon contains high abundances of Pb*, which also allows for better counting statistics during measurement. Variations in Pb^*/Pb_c are dependent upon the [U] of a zircon, the duration of radiogenic in-growth and the procedural lab blank, and as a result can vary significantly between data sets and different labs. In addition, the data compiled in Fig. 4 may represent lower uncertainties in U-Pb measurement relative to other data compilations, as analytical Pb fractionation was corrected during measurement using the ET2535 spike, and U isotope compositions were precisely measured on Faraday collectors coupled 10^{12} Ω resistance amplifiers. Due to the high preci-

sion of the analyses presented here, it is possible to identify discordance and interpret the data array by two-component mixing of zircon domains that formed during two geologically separate periods of crystallization (Fig. 3). Most commonly, data sets that consist of lower-precision analyses are not capable of resolving concordance vs. discordance at the same level of precision (e.g., older $^{205}Pb/^{235}U$ spiked ID-TIMS dates, as in Schaltegger and Corfu, 1992, LA-ICPMS or SIMS dates). As a result, a population of data with different but overlapping $^{206}Pb/^{238}U$ dates at lower precision may be analytically concordant and erroneously interpreted in terms of protracted autocrystic growth, while the population actually reflects mixing of two disparate age domains.

To illustrate the potential for individual analyses to yield concordant results at low level of precision falsely mimicking protracted crystallization, we calculated two models of two-component mixing, (1) based on the data from 676PA aliquot and (2) of a hypothetical Miocene igneous rock with xenocrystic inheritance.

5.2.1. Model 1

The aliquot of the Punteglias granodiorite with a weaker physical abrasion (676PA) yielded both concordant and discordant ages and no overlapping analyses, however the ability to resolve those features is due to the low uncertainties. These analyses had high Pb^*/Pb_c compositions of 153–536 (Fig. 5; Table S1). To demonstrate how decreased precision will lead to apparent concordance and overlap within this dataset, we recalculated the actual analyses (black uncertainty ellipses in Fig. 5) with parameters more commonly observed in U-Pb zircon geochronology, i.e., with the uncertainties associated with a Pb^*/Pb_c of 50 (blue ellipses) and of 10 (red ellipses; Fig. 5). Lower Pb^*/Pb_c leads to a dramatic increase mainly of the $^{207}Pb/^{235}U$ uncertainties but also affects the $^{206}Pb/^{238}U$ uncertainties (Fig. 4). This simulation shows that every measurement would have been concordant within uncertainty, and there would be overlap between several of the oldest analyses if the analyses of aliquot 676PA were generated at a lower level of radiogenic Pb or a higher level of common Pb abundance (blank), such as those with a Pb^*/Pb_c ratio of 10. In such a scenario, a potentially preferred interpretation would be that the parental magma system that formed the Punteglias granodiorite may have had a lifespan of 10.784 ± 0.658 Myr, interpreting the protracted concordant analyses to reflect antecrystic inheritance and/or protracted autocrystic growth. Applying an average uncertainty associated with a Pb^*/Pb_c of 50, all except for the youngest analyses would still be concordant, although none of the $^{206}Pb/^{238}U$ dates would overlap within uncertainty. Using a similar interpretive logic, this sample could have been interpreted to reflect a magma system with a lifespan of 6.105 ± 0.265 Myr. Interpreting these age ranges to reflect antecrystic inheritance mixed with autocrystic zircon ages would indicate an overall long-lived magmatic system, but this interpretation does not necessitate that the magmatic system was active for that entire period. In the measured data set, only the oldest five analyses were concordant and none of the analyses overlap, but most importantly these data yield a linear relationship indicative of two-component mixing, and therefore require a totally different model for determining the significance of the age spectra. In conclusion, natural data sets representing these three examples would be interpreted in very different ways, in spite of having the same absolute ages, due to differing uncertainties applied.

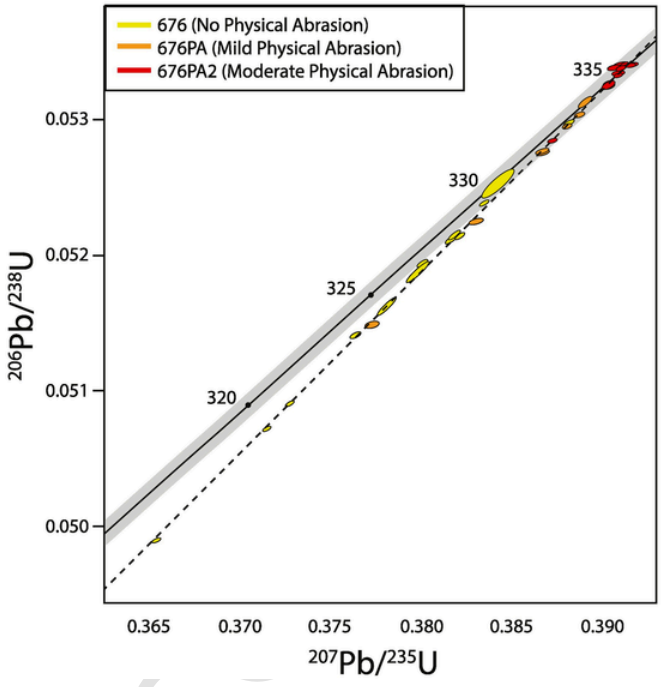

Fig. 3. Zircon U-Pb CA-ID-TIMS results from sample KAW676 of the Punteglias Granodiorite separated into separate aliquots that all underwent 12 h chemical abrasion but different degrees of physical abrasion, displayed on a Weatherill concordia. The dashed line on the concordia diagram is a Discordia line calculated using all grains analyzed by CA-ID-TIMS in this study, and yields an upper intercept value of 334.6 ± 0.60 Ma and a lower intercept of 24 ± 11 Ma (MSWD = 5.2, n = 32). The aliquot of 676 with no physical abrasion (676) shows significant dispersion down the Discordia line, whereas the aliquot with the most physical abrasion (676PA2) only yielded analyses which were concordant within uncertainty with an overlapping cluster at approximately 335.5 Ma. The interpreted zircon crystallization age of this sample of the Punteglias granite is 335.479 ± 0.041/0.096/0.37 Ma, based on calculating a weighted mean age of this plateau of ages from aliquot 676PA2. See text for discussion.

5.2.2. Model 2

Mixing of igneous, autocrystic zircon with older components of variable age (e.g., antecrysts or xenocrysts) in young magmatic systems is distinct from the above case of mixing of igneous cores with younger metamorphic rims from the Punteglias granodiorite. We present here an alternative, synthetic model of a hypothetical 25 Ma igneous rock in which all autocrystic zircon crystallized instantaneously, but inherited inclusions of 250 Ma zircon, with varied $[U]_{autocryst}/[U]_{inclusion}$ of 0.25, 1 and 4 (Fig. 6A, B, C). This example of two component mixing is more applicable to rocks with a purely igneous history, particularly in commonly studied Cenozoic rocks. The volumetric percentage of xenocrystic inclusions varies from 0 to 1% in Fig. 6. The synthetic data are presented with uncertainties associated with Pb^*/Pb_c of 10, 50 and 100, with an average uncertainty taken from Fig. 4, to further illustrate the significance of precision on the ability to assess potential two-component mixing in U-Pb data.

This synthetic data set yields a range of both concordant and discordant data, with the degree of overlap and concordance largely a function of uncertainty of analysis and to the mixing proportion of $[U]_{autocryst}/[U]_{inheritance}$. Two-component mixing in concordia space is fixed between the two end member dates of 25 and 250 Ma on concordia, and therefore the range of mixing solutions which yield a value overlapping with concordia is defined by the precision of individual analyses mostly of the $^{207}Pb/^{235}U$ ratios. For data generated with the uncertainty associated with Pb^*/Pb_c of 100 (from Fig. 4), concordant $^{206}Pb/^{238}U$ dates range from 25.0000 ± 0.0037 to 25.8113 ± 0.0039 Ma (Δt = 0.8113 ± 0.0076 Ma). Using the uncertainties associated with a composition of Pb^*/Pb_c = 50, the range of concordant $^{206}Pb/^{238}U$ dates extends up to 26.164 ± 0.005 Ma (Δt = 1.164 ± 0.010 Ma), and for the uncertainties associated with a Pb^*/Pb_c of 10 it further extends to 29.065 ± 0.015 Ma (Δt = 4.065 ± 0.028 Ma). Therefore, the ability to detect two-component mixing with an ancient source based upon normal discordance is dependent on the precision of individual analyses. It is worth acknowledging here that compositions of Pb^*/Pb_c of 100 are unrealistic

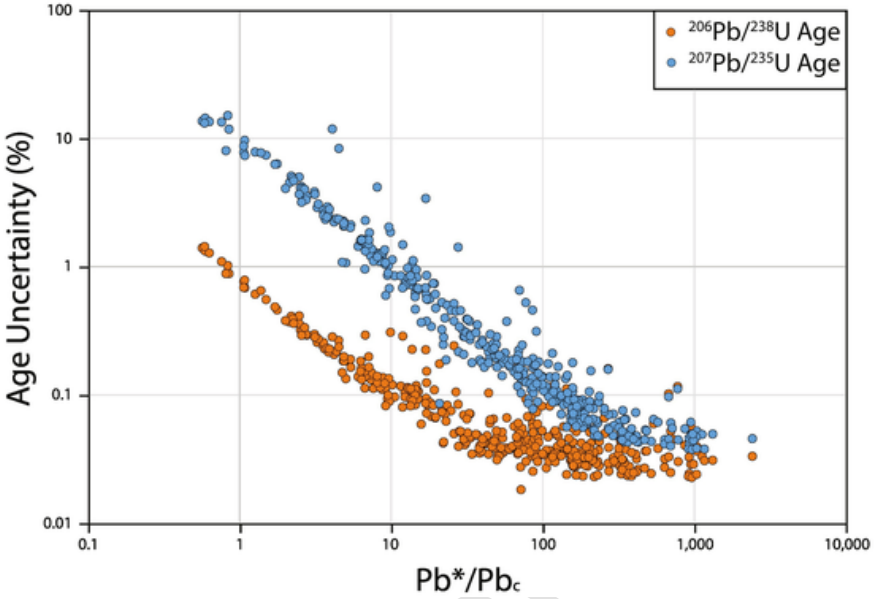

Fig. 4. Zircon isotope data of CA-ID-TIMS analyses of natural samples spiked with the ET2535 tracer solution analyzed on the University of Geneva IsotopX Phoenix TIMS between 2019 and 2021, highlighting the difference in uncertainties between $^{206}Pb/^{238}U$ and $^{207}Pb/^{235}U$ ages based on varying Pb^*/Pb_c compositions. Both axes are plotted on a logarithmic scale. Figure includes data from Brlek et al. (2020), Greber et al. (2020), Schaltegger et al. (2021a), Schaltegger et al. (2021b) Brlek et al. (2021), Gaynor et al. (2022), this study and unpublished data.

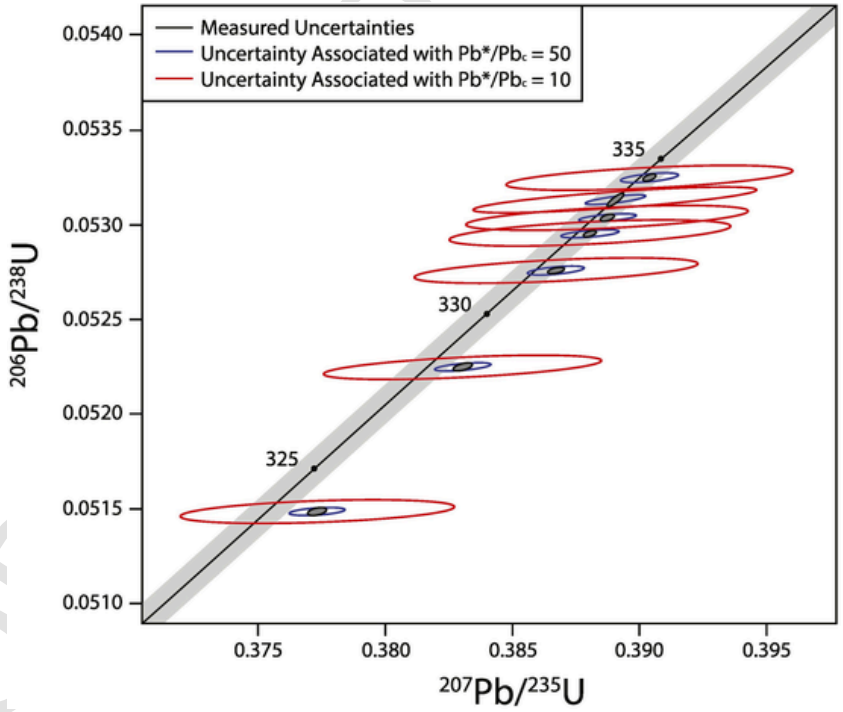

Fig. 5. Comparison of how variations in Pb^*/Pb_c can influence the ability for individual analyses to be analytically concordant, using the measured $^{206}Pb/^{238}U$ and $^{207}Pb/^{235}U$ ratios of measured aliquots of 676PA, and comparing the measured uncertainties to those which could be expected with Pb^*/Pb_c values of 50 and 10. At lower Pb^*/Pb_c values, the significantly higher $^{207}Pb/^{235}U$ uncertainties lead to apparent analytical concordance, allowing for the ability to obfuscate inaccurate $^{206}Pb/^{238}U$ crystallization ages via multicomponent mixing. See text for further discussion.

for most 25 Ma zircon, Pb^*/Pb_c of 5–50 are far more likely in this age range due to limited radiogenic Pb in-growth, and therefore the ability to perceive mixing for a hypothetical 25 Ma sample may be quite limited in natural samples of this age. Assuming that protracted magmatic growth of zircon would generally last within a maximum time frame of a million years, a conclusive distinction between protracted magmatic crystallization and two-component mixing on individual dates cannot be reasonably made on the isotopic data alone if Pb^*/Pb_c ratio = 50, assuming similar uncertainties to those presented in Fig. 4.

Another aspect worth considering is the relative size of inclusions: thorough prescreening of sectioned zircon grains may potentially identify xenocrystic cores if there is sufficient volume of xenocrystic material present and if the zircon cross section exposed in the grain mount intersects the xenocrystic inclusion. The higher the relative concentration of U in the xenocrystic component, the easier it is for a volumetrically

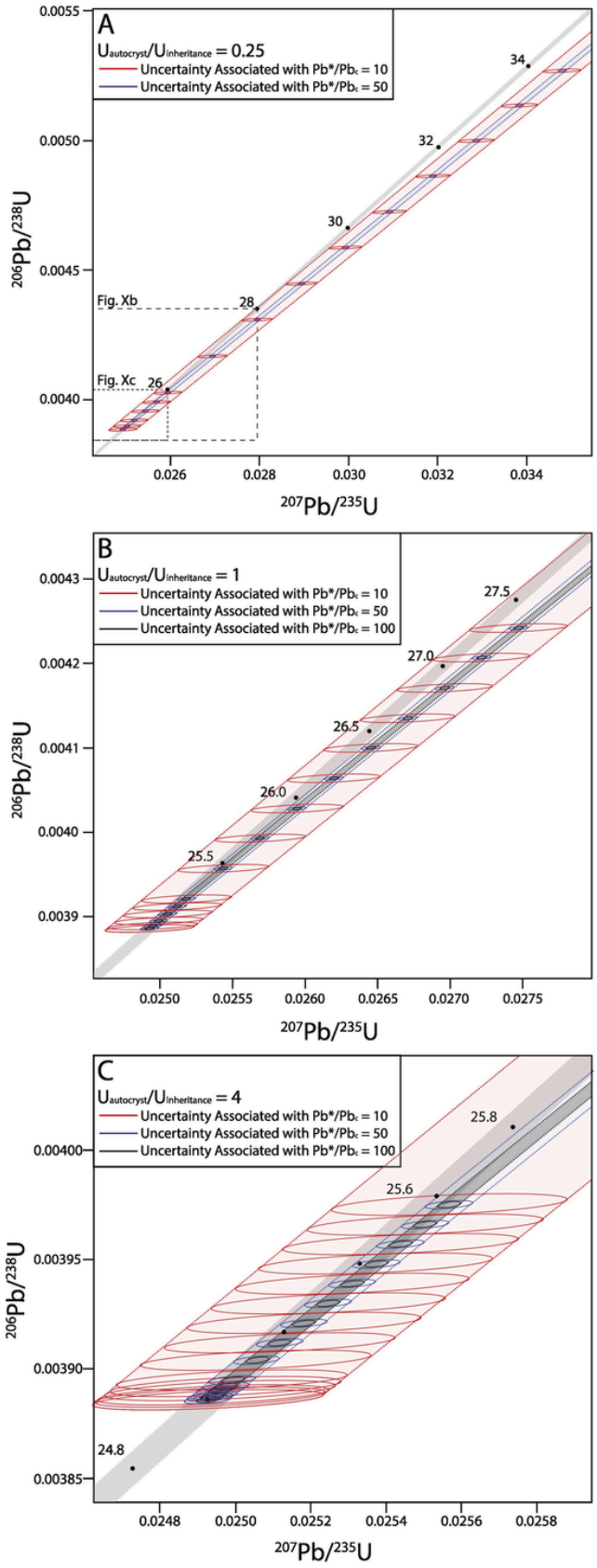

Fig. 6. Two component mixing model, mixing 25 Ma old autocrystic zircon with 250 Ma old xenocrystic material, highlighting the expected analytical uncertainty of these potential mixing solutions analyzed via ID-TIMS with Pb^*/Pb_c values of 10, 50 and 100. Individual ellipses plotted on each diagram correspond to various mixing solutions ranging from 0.0001–1% volume percentage of inherited volume within the 25 Ma zircon crystal. At lower Pb^*/Pb_c values, the significantly higher $^{207}Pb/^{235}U$ uncertainties lead to apparent analytical concordance, allowing for the ability to obfuscate inaccurate $^{206}Pb/^{238}U$ crystallization ages via multicomponent mixing. Therefore, it is unlikely that protracted magmatic (autocrystic) growth can be directly assessed from ID-TIMS measurements with lower with Pb^*/Pb_c compositions without additional complimentary data. See text for further discussion.

smaller inclusion to significantly affect the age of a zircon. As shown in Fig. 6 and Fig. S2, a small proportion of high-U inclusion may bias ID-TIMS ages without necessarily being detectable through CL imaging prior to analysis.

5.3. How complex U-Pb systematics impact the accuracy of geological models

Our synthetic model of randomly sampled individual data points may resemble an extended, high-precision zircon age spectrum generated from some natural samples (Fig. 6). In such a natural case, we may identify a certain duration of zircon crystallization through protracted autocrystic crystallization and/or antecrystic inheritance, by assuming there is no incorporation of a xenocrystic component. This would be the preferred hypothesis by many authors, using this to explain the intrinsic characteristics of a given magmatic system in terms of duration, tempo and emplacement rate of magma. This interpretation will also allow for calculating an age of eruption or of plutonic solidification. However, all of this attaches significant genetic connotations to the nature of individual zircon ages, which need to be demonstrated to support the initial hypothesis. Contrarily, in our model autocrystic crystallization is instantaneous and therefore the variation of data points along the Concordia is due to mixing of two age components and does not support any connotation of protracted or diachronous zircon growth.

By interpreting protracted U-Pb zircon age spectra in igneous rocks we infer which mechanisms were active during zircon crystallization, which reflect on the history on the crystallizing melt volume as well as on the magmatic system as a whole. A system producing only *autocrystic zircon* will yield a range of zircon dates that reflect duration of zircon crystallization. From crystal size and age distribution we can simulate the integrated volume of zircon crystallizing in space and time (Caricchi et al., 2014, 2016), and track the thermal evolution of a magma after zircon saturation by combining U-Pb dates with geochemical information (e.g., Samperton et al., 2017). A system which includes *antecrystic zircon* components will record an antecedent magma history preceding the formation of the volume of magma sampled for zircon analysis, such that the zircon age spectrum will reflect the history of a larger portion of the magmatic system. Finally, a system may incorporate *xenocrystic components* from the anatectic source, or from a structural level of magma residence, and then utilizes this material as a nucleation point for subsequent crystallization of autocrystic zircon. In this case, the overall age dispersion in concordant analyses observed in an individual sample may not have significance towards a rock's magmatic history. However, depending on analytical precision and age of mixing end members, all three of these mechanisms can yield a range of concordant zircon dates. Assigning a specific interpretation to such a data set without additional constraints can lead to a fundamentally wrong interpretation or model for a specific magmatic system. Therefore, our data set of 676PA analyses and our synthetic models presented above highlight the necessity of high precision measurements of zircon geochronology to arrive at the most correct interpretation of complex age spectra.

Finally, an additional component to consider is Pb-loss, where incomplete pretreatment or a lack of chemical pretreatment causes inclusion of younger crystallographic domains into analysis. While recent research has demonstrated that prolonged chemical abrasion at high tem-

perature can largely mitigate the effects of Pb-loss (e.g., Widmann et al., 2019; Keller et al., 2019), high-U and/or old zircon may not be robust enough to withstand full chemical abrasion pretreatment (e.g., Lantink et al., 2019; Gaynor et al., 2022). Furthermore, the hydrothermal-magmatic alteration observed in many porphyry deposits can induce Pb-loss, which cannot be readily mitigated by thorough chemical abrasion (e.g., Gaynor et al., 2019b; Rosera et al., 2021).

There are several techniques that can be used in tandem with high-precision geochronology to improve the validity of geologic interpretations. Combining other isotope analyses, such as Hf or O isotopes, of the volume of zircon dated by ID-TIMS can be used to reveal geologic mechanisms behind complicated dates (e.g., Davies et al., 2021; Gaynor et al., 2022). For zircon with complicated metamorphic histories, physical abrasion prior to chemical abrasion is very useful and presently underutilized tool to remove overgrowth domains to allow for more accurate dating of primary igneous crystallization, such as shown in this study and by numerous studies in the past (e.g., Corfu et al., 1989; Schaltegger and Corfu, 1992). Finally, microsampling crystals to date individual zones or domains through physically breaking them or dissecting them with a either a laser or a FIB is a precise method to determine the potential growth histories of individual grains (e.g., Samperton et al., 2015; Kovacs et al., 2020; White et al., 2020). Combining high-precision ages with additional data and isolating or removing discrete crystallographic domains is a strong way to bolster geologic interpretations of complicated data.

6. Conclusions

Zircon geochronology of the Punteglias granodiorite shows the potential for complications inherent with many modern, high-precision U-Pb datasets. The CA-ID-TIMS data show a two-component mixing relationship, with trace volumes of younger zircon domains causing some linear dispersion in the data in Concordia space. We conclude that it is dangerous to infer a geologic model from complicated U-Pb zircon age spectra based on the criterion of concordance alone, particularly from analyses with a less precise $^{207}Pb/^{235}U$ date. Antecrystic or xenocrystic inclusions can bias the $^{206}Pb/^{238}U$ dates towards older values without becoming normally discordant, while unresolved young overgrowth may bias a magmatic age towards younger values. These complications are present in all analytical data sets, including less precise in-situ U-Pb analyses employing LA-ICPMS and SIMS techniques, therefore careful evaluation of any protracted age spectra and unbiased discussion are necessary for proper geologic interpretation. Favoring the interpretation of prolonged crystallization over two-component mixing thus remains hypothetical at the levels of precision commonly obtained, unless other supportive arguments can be raised such isotopic or trace element information from analyzed zircon or by high-precision temporal resolution derived from subsampling individual zircon crystals.

Uncited reference

Declaration of Competing Interest

The authors declare that they have no known competing financial interests or personal relationships that could have appeared to influence the work reported in this paper.

Acknowledgments

This research was supported by the Swiss National Science Foundation project No. 200020_182007 to U.S. Jean-Marie Boccard helped with mount preparation of the zircons and SEM imagery was supported by Agathe Martignier. Thanks to Editor-in-Chief Catherine Chauvel for the handling and feedback of this manuscript, as well as to Fernando Corfu and an anonymous reviewer for thorough, constructive reviews of this manuscript.

Appendix A. Supplementary data

Supplementary data to this article can be found online at https://doi.org/10.1016/j.chemgeo.2022.120913.

References

Berger, A., Wehrens, P., Lanari, P., Zwingmann, H., Hrwegh, M., 2017. Microstructures, mineral chemistry and geochronology of white micas along a retrograde evolution: an example from the Aar massif (Central Alps, Switzerland). Tectonophysics 721, 179–195.

Bowring, J.F., McLean, N.M., Bowring, S.A., 2011. Engineering cyber infrastructure for U-Pb geochronology: tripoli and U-Pb_Redux. Geochem. Geophys. Geosyst. 12, 19.

Brlek, M., Kutterolf, S., Gaynor, S.P., Kuiper, K., Belak, M., Brčić, V., Holcová, K., Wang, K.L., Bakrač, K., Hajek-Tadesse, V., Mišur, I., Horvat, M., Šuica, S., Schaltegger, U., 2020. Miocene syn-rift evolution of the North Croatian Basin (Carpathian-Pannonian Region): new constraints from Mts. Kalnik and Požeška gora pyroclastic and sedimentary record with regional implications. Int. J. Earth Sci. 109, 2775–2800.

Brlek, M., Gaynor, S.P., Bauluz, B., Sinisi, R., Mongelli, G., Brčić, V., Peytcheva, I., Mišur, I., Tapster, S., Ilijanić, A., Kukoč, D., Schaltegger, U., 2021. Karst bauxite formation during Miocene Climatic Optimum (Central Dalmatia, Croatia): mineralogical, compositional and geochronological perspectives. Int. J. Earth Sci. 110, 1466–1477.

Caricchi, L., Simpson, G., Schaltegger, U., 2014. Zircons reveal magma fluxes in Earth's crust. Nature 511, 457–461.

Caricchi, L., Simpson, G., Schaltegger, U., 2016. Estimates of volume and magma input in crustal magmatic systems from zircon geochronology: the effect of modeling assumptions and system variables. Front. Earth Sci. v. 4, 15.

Challandes, N., Marquer, D., Villa, I.M., 2008. P-T-t modelling, fluid circulation, and ^{39}Ar-^{40}Ar and Rb-Sr mica ages in the Aar Massif shear zones (Swiss Alps). Swiss J. Geosci. 101, 269–288.

Condon, D.J., Schoene, B., McLean, N.M., Bowring, S.A., Parrish, R.R., 2015. Metrology and traceability of U–Pb isotope dilution geochronology (EARTHTIME Tracer Calibration Part I). Geochim. Geochim. Cosmochim. Acta 164, 464–480.

Corfu, F., Krogh, T.E., Kwok, Y.Y., Jensen, L.S., 1989. U-Pb zircon geochronology in the southwestern Abitibi greenstone belt, Superior Province. Can. J. Earth Sci. 26, 1747–1763.

Curry, A.C., Gaynor, S.P., Davies, J.H.F.L., Ovtcharova, M., Simpson, G., Caricchi, L., 2021. Evidence for Prolonged Magma Assembly Leading to an Ignimbrite Flare-Up in the San Juan Mountains. Contributions to Mineralogy and Petrology, v, Colorado, p. 176.

Davies, J.H.F.L., Marzoli, A., Bertrand, H., Youbi, N., Ernesto, M., Greber, N.D., Ackerson, M., Simpson, G., Bouvier, A.S., Baumgartner, L., Pettke, T., Farina, F., Ahrenstedt, H.V., Schaltegger, U., 2021. Zircon petrochronology in large igneous provinces reveals upper crustal contamination processes: new U-Pb ages, Hf and O isotopes, and trace elements from the Central Atlantic magmatic province (CAMP). Contrib. Mineral. Petrol. v. 176.

Gaynor, S.P., Coleman, D.S., Rosera, J.M., Tappa, M.J., 2019a. Geochronology of a bouguer anomaly. J. Geophys. Res. Solid Earth 124, 2457–2468.

Gaynor, S.P., Rosera, J.M., Coleman, D.S., 2019b. Magmatic history of the Questa Mo Porphyry Deposit. Geosphere 15, 548–575.

Gaynor, S.P., Svensen, H., Polteau, S., Schaltegger, U., 2022. Local melt contamination and global climate impacts: dating the emplacement of Karoo LIP sills in organic-rich shale. Earth Planet. Sci. Lett. 579, 117371.

Greber, N., Davies, J.H.F.L., Gaynor, S.P., Schaltegger, U., Jourdan, F., Bertrand, H., 2020. Constraining age of emplacement and environmental impact of the Karoo large igneous province by high-precision U-Pb ages and Hf isotope data: results. Geochemistry 1, 8.

Hiess, J., Condon, D.J., McLean, N., Noble, S.R., 2012. $^{238}U/^{235}U$ systematics in terrestrial uranium-bearing minerals. Science v., 335, 1610–1614.

Janots, E., Rubatto, D., 2014. U-Th-Pb dating of collision in the external Alpine domains (Urseren zone, Switzerland) using low temperature allanite and monazite. Lithos v. 184–187, 155–166.

Janoušek, V., Hanzl, P., Svojtka, M., Hora, J.M., Kochergina, Y.V.E., Gadas, P., Holub, F.V., Gerdes, A., Verner, K., Hrdlicková, K., Daly, J.S., Buriánek, D., 2020. Ultrapotassic magmatism in the heyday of the Variscan Orogeny: the story of the Třebíč Pluton, the largest durbachitic body in the Bohemian Massif. Int. J. Earth Sci. 109, 1767–1810.

Keller, C.B., Boehnke, P., Schoene, B., Harrison, T.M., 2019. Stepwise chemical abrasion-isotope dilution-thermal ionization mass spectrometry with trace element analysis of microfractured Hadean zircon. Geochronology 1, 85–97.

Kovacs, N., Allan, M.M., Crowley, J.L., Colpron, M., Hart, C.J.R., Zagorevski, A., Creaser, R.A., 2020. Carmacks Copper Cu-Au-Ag deposit: Mineralization and postore migmatization of a Stikine Arc porphyry copper system in Yukon, Canada. Econ. Geol. v. 115, 1413–1442.

Krogh, T.E., 1973. A low-contamination method for hydrothermal decomposition of zircon and extraction of U and Pb for isotopic age determinations. Geochim. Cosmochim. Acta 37, 485–494.

Lantink, M.L., Davies, J.H.F.L., Mason, P.R.D., Schaltegger, U., Hilgen, F.J., 2019. Climate control on banded iron formation linked to orbital eccentricity. Nat. Geosci. 12, 369–374.

Large, S.J.E., Buret, Y., Wotzlaw, J.F., Karakas, O., Guillong, M., von Quadt, A., Heinrich, C.A., 2021. Copper-mineralised porphyries sample the evolution of a large-volume silicic magma reservoir from rapid assembly to solidification. Earth Planet. Sci. Lett. 563, 12.

Marquer, D., Burkhard, M., 1992. Fluid circulation, progressive deformation and mass-transfer processes in the upper crust: the example of basement-cover relationships in the External Crystalline Massifs, Switzerland. J. Struct. Geol. 14, 1047–1057.

Mattinson, J.M., 2005. Zircon U–Pb chemical abrasion ("CA-TIMS") method: combined annealing and multi-step partial dissolution analysis for improved precision and accuracy of zircon ages. Chem. Geol. 220, 47–66.

McLean, N.M., Bowring, J.F., Bowring, S.A., 2011. An algorithm for U–Pb isotope dilution data reduction and uncertainty propagation. Geochem. Geophys. Geosyst. 12, 26.

McLean, N.M., Condon, D.J., Schoene, B., Bowring, S.A., 2015. Evaluating uncertainties in the calibration of isotopic reference materials and multi-element isotopic tracers (EARTHTIME Tracer Calibration Part II). Geochim. Cosmochim. Acta 164, 481–501.

Miller, J.S., Matzel, J.E.P., Miller, C.F., Burgess, S.D., Miller, R.B., 2007. Zircon growth and recycling during the assembly of large, composite arc plutons. J. Volcanol. Geotherm. Res. 167, 282–299.

Mundil, R., Ludwig, K.R., Metcalf, I., Renne, P.R., 2004. Age and timing of the Permian mass extinctions: U/Pb dating of closed-system zircons. Science 305, 669–673.

Murakami, T., Chakoumakos, B.C., Ewing, R.C., Lumpkin, G.R., Weber, W.J., 1991. Alpha-decay event damage in zircon. Am. Mineral. 76, 1510–1532.

Pidgeon, R.T., 2014. Zircon radiation damage ages. Chem. Geol. 367, 13–22.

Rivera, T.A., Schmitz, M.D., Jicha, B.R., Crowley, J.L., 2016. Zircon petrochronology and 40Ar/39Ar sanidine dates for the Mesa Falls Tuff: Crystal-scale records of magmatic evolution and the short lifespan of a large Yellowstone magma chamber. J. Petrol. 57, 1677–1704.

Rolland, Y., Cox, S.F., Corsini, M., 2009. Constraining deformation stages in brittle-ductile shear zones from combined field mapping and ^{40}Ar-^{39}Ar dating: the structural evolution of the Grimsel Pass area (Aar Massif, Swiss Alps). J. Struct. Geol. 31, 1377–1394.

Rosera, J.M., Gaynor, S.P., Coleman, D.S., 2021. Spatio-temporal shifts in magmatism and mineralization in Northern Colorado beginning in the late Ecocene. Econ. Geol. 116, 987–1010.

Ruiz, M., Schaltegger, U., Gaynor, S.P., Chiaradia, M., Abrecht, J., Gisler, C., Giovanoli, F., Wiederkehr, M., In revision, reassessing the intrusive tempo and magma genesis of the late Variscan Aar batholith through zircon U-Pb geochronology and Hf isotopes: Swiss J. Geosci.

Samperton, K.M., Schoene, B., Cottle, J., Keller, C.B., Crowley, J.L., Schmitz, M.D., 2015. Magma emplacement, differentiation and cooling in the middle crust: Integrated zircon geochronological-geochemical constraints from the Bergell Intrusion. Centr. Alps Chem. Geol. 417, 322–340.

Samperton, K.M., Bell, E.A., Barboni, M., Keller, C.B., Schoene, B., 2017. Zircon age-temperature-compositional spectra in plutonic rocks. Geology 45, 983–986.

Schaltegger, U., 1997. Magma pulses in the Central Variscan Belt: episodic melt generation and emplacement during lithospheric thinning. Terra Nova 9, 242–245.

Schaltegger, U., Corfu, F., 1992. The age and source for late Hercynian magmatism in the Central Alps: evidence from precise U-Pb ages and initial Hf isotopes. Contrib. Mineral. Petrol. 111, 329–344.

Schaltegger, U., Corfu, F., 1995. Late Variscan "Basin and Range" magmatism and tectonics in the Central Alps: evidence from U-Pb geochronology. Geodin. Acta 8, 82–98.

Schaltegger, U., Gaynor, S.P., Widmann, P., Kotková, J., 2021b. Comment on "Ultrapotassic magmatism in the heyday of the Variscan Orogeny: the story of the Třebíč Pluton, the largest durbachitic body in the Bohemian Massif" by Janoušek et al. Int. J. Earth Sci. 110, 1127–1132. https://doi.org/https://.org/10.1007/s00531-020-01975-w.

Schaltegger, U., Ovtcharova, M., Gaynor, S.P., Schoene, B., Wotzlaw, J., Davies, J.H.F.L., Farina, F., Greber, N., Szymanowski, D., Chelle-Michout, C., 2021a. Long-term repeatability and interlaboratory reproducibility of high-precision ID-TIMS U-Pb geochronology. J. Anal. At. Spectrom. 36, 1466–1477.

Schaltegger, U., von Quadt, A., 1990. U-Pb zircon dating of the Central Aar Granite (Aar Massif, Switzerland): Schweiz Mineral. Petrogr. Mitt. 70, 361–371.

Schaltegger, U., Corfu, F., Krogh, T.E., 1991. Precise U-Pb ages and initial Hf isotopic compositions of late Hercynian mafic to acid intrusives in the Aar Massif, Central Alps. Terra Abstracts 3, 37.

Schoene, B., Eddy, M.P., Samperton, K.M., Keller, C.B., Keller, G., Adatte, T., Khadri, S.F.R., 2019. U-Pb constraints on pulsed eruption of the Deccan Traps across the end-cretaceous mass extinction. Science 363, 862–866.

Schulmann, K., Lexa, O., Janoušek, V., Lardeaux, J.M., Edel, J.B., 2014. Anatomy of a diffuse cryptic suture zone: an example from the Bohemian Massif. Europ. Varisc. Geol. 42, 275–278.

Seeman, U., 1975. Mineralogisch-petrographische und geochemische Untersuchungen der granitischen Gesteine der Val Punteglias (GR): Schweiz. Mineral. Petrogr. Mitt. 55, 257–306.

Szymanowski, D., Schoene, B., 2020. U-Pb ID-TIMS geochronology using ATONA amplifiers. J. Anal. At. Spectrom. 35, 1207–1216.

Tapster, S., Condon, D.J., Naden, J., Noble, S.R., Petterson, M.G., Roberts, N.M.W., Saunders, A.D., Smith, D.J., 2016. Rapid thermal rejuvenation of high-crystallinitiy magma linked to porphyry copper deposit formation; evidence from the Koloula Porphyry Prospect, Solomon Islands. Earth Planet. Sci. Lett. 442, 206–217.

Vanderhaeghe, O., Laurent, O., Gardien, V., Moyen, J.F., Gébelin, A., Chelle-Michou, C., Couzinié, S., Villaros, A., Bellanger, M., 2020. Flow of partially molten crust controlling construction, growth and collapse of the Variscan orogenic belt: the geologic record of the French Massif Central. Bull. Soc. Géol. France v. 191, 25.

von Quadt, Wotzlaw J.F., Buret, Y., Large, S.J.E., Peytcheva, I., Trinquier, A., 2016. High-precision zircon U/Pb geochronology by ID-TIMS using new 10^{13} ohm resistors. J. Anal. At. Spectrom. 31, 658–665.

von Raumer, J.F., Bussy, F., Schaltegger, U., Schulz, B., Stampfli, G.M., 2013. Pre-Mesozoic Alpine basements- their place in the European Paleozoic framework. GSA Bull. 125, 89–108.

Wehrens, P., Baumberger, R., Berger, A., Herwegh, M., 2017. How is strain localized in a meta-granitoid, mid-crustal basement section? Spatial distribution of deformation in the central Aar massif (Switzerland). J. Struct. Geol. 94, 47–67.

White, L.F., Tait, K.T., Kamo, S.L., Moser, D.E., Darling, J.R., 2020. Highly accurate dating of micrometer-scale baddeleyite domains through combined focus ion beam extraction and U-Pb thermal ionization mass spectrometry (FIB-TIMS). Geochronology v. 2, 177–186.

Widmann, P., Davies, J.H.F.L., Schaltegger, U., 2019. Calibrating chemical abrasion: its effects on zircon crystal structure, chemical composition and U-Pb age. Chem. Geol. 511, 1–10.

Wotzlaw, J.F., Schaltegger, U., Frick, D.A., Dungan, M.A., Gerdes, A., Günther, D., 2013. Tracking the evolution of large-volume silicic magma reservoirs from assembly to supereruption. Geology 41, 867–870.